An Effective Radius Retrieval for Thick Ice Clouds Using GOES

DANIEL T. LINDSEY

Regional and Mesoscale Meteorology Branch, NOAA/NESDIS, Fort Collins, Colorado

LOUIE GRASSO

Cooperative Institute for Research in the Atmosphere, Fort Collins, Colorado

(Manuscript received 5 October 2006, in final form 13 August 2007)

ABSTRACT

Satellite retrieval of cirrus cloud microphysical properties is an important but difficult problem because of uncertainties in ice-scattering characteristics. Most methods have been developed for instruments aboard polar-orbiting satellites, which have better spatial and spectral resolution than geostationary sensors. The Geostationary Operational Environmental Satellite (GOES) series has the advantage of excellent temporal resolution, so that the evolution of thunderstorm-cloud-top properties can be monitored. In this paper, the authors discuss the development of a simple ice cloud effective radius retrieval for thick ice clouds using three bands from the GOES imager: one each in the visible, shortwave infrared, and window infrared portion of the spectrum. It is shown that this retrieval compares favorably to the MODIS effective radius algorithm. In addition, a comparison of the retrieval for clouds viewed simultaneously from GOES-East and GOES-West reveals that the assumed ice-scattering properties perform very well. The algorithm is then used to produce maps of mean ice cloud effective radius over the continental United States. A real-time version of this retrieval is currently running and may be used to study the evolution of thunderstorm-top ice crystal size in rapidly evolving convection.

1. Introduction

Cirrus cloud microphysical properties, like optical depth and effective radius, have received much attention in the literature due to their important role in regulating climate (e.g., Liou 1986; Stephens et al. 1990; Cooper et al. 2006). A great majority of satellite retrievals of these parameters has been developed for instruments aboard polar-orbiting satellites, such as the Moderate Resolution Imaging Spectroradiometer (MODIS) and the Advanced Very High Resolution Radiometer (AVHRR), but fewer studies have developed retrieval techniques for instruments in geostationary orbit (e.g., Han et al. 1994; Roebeling et al. 2006). This is likely due to the limited spatial and spectral resolution available on geostationary sensors. However, instruments such as the imager aboard the current generation of Geostationary Operational Environmental Satellites (GOES) have excellent temporal resolution, allowing for scans approximately 7 min apart during Rapid Scan Operation (RSO). This allows the evolution of many weather features (such as thunderstorms and tropical storms) that change on short time scales to be monitored. Lindsey et al. (2006) hypothesize that thunderstorm-top ice crystal size is related to updraft strength, so an effective radius retrieval with GOES may have practical nowcasting applications.

Nakajima and King (1990) introduce a method for determining optical thickness and effective radius from a band in the visible and a band in the shortwave infrared (IR) portion of the spectrum. They show that visible reflectance varies mostly with optical thickness, while shortwave IR reflectance varies primarily with effective radius. For clouds having large optical thicknesses, effective radius can be determined with the shortwave IR band alone (e.g., Wetzel et al. 1996). This method works quite well with liquid water clouds due to the predictable scattering properties of cloud droplets, but ice clouds are much more complex due to differing habits and irregular crystal shapes. Minnis et al. (1993) introduce a satellite method to retrieve cirrus

Corresponding author address: Daniel T. Lindsey, CIRA/Colorado State University, 1375 Campus Delivery, Fort Collins, CO 80523-1375.
E-mail: lindsey@cira.colostate.edu

DOI: 10.1175/2007JAMC1612.1

cloud properties using visible and IR radiances, but their primary goal is obtaining cloud altitude and optical depth, not particle size. McKague and Evans (2002) describe a retrieval technique for various cloud parameters, including ice crystal size, using radiances from the GOES imager. Their method retrieves cloud parameter probability density functions, as opposed to pixel-by-pixel values, and is most useful for evaluating global climate model cloud parameterizations. Recently, a number of studies have attempted to better document the scattering properties of nonspherical ice crystals (e.g., Yang et al. 2000, 2003, 2005). Baum et al. (2005a) use in situ data collected during a number of field experiments, along with the scattering properties of several ice crystal habits to develop a "recipe" for habit mixtures as a function of crystal size. This information can then be used to make forward model calculations of cloud radiative properties (e.g., Baum et al. 2005b), which in turn can be used to develop a satellite retrieval method. Cooper et al. (2006) perform an information content analysis to determine what combination of spectral measurements yield the best ice cloud effective radius retrieval. They suggest using a five-channel approach; however, given the limited number of channels available on the GOES imager, a simpler retrieval is necessary. The GOES imager has five channels, three of which are used in this retrieval algorithm: band 1 (0.65 μm, visible, 1-km resolution), band 2 (3.9 μm, shortwave IR, 4-km resolution), and band 4 (10.7 μm, window IR, 4-km resolution).

This study uses ice-scattering properties along with an observational operator to develop an effective radius retrieval for optically thick ice clouds using GOES. The retrieval has a number of distinct advantages: 1) it uses the most sophisticated (to date) set of ice-scattering properties, 2) the use of a lookup table allows the retrieval to be performed in real time due to relatively few necessary computations, and 3) it is restricted to thick ice clouds, so errors associated with transmittance and surface albedo are avoided altogether. Section 2 describes the model and the method used to generate lookup tables; section 3 provides some error estimates and validation procedures; and section 4 offers a summary.

2. Forward model calculations

The observational operator (Greenwald et al. 2002; Grasso and Greenwald 2004) used for the forward model calculations makes use of the plane-parallel version of the Spherical Harmonic Discrete Ordinate Method (SHDOM; Evans 1998), subsequently referred to as SHDOMPP. A homogeneous cloud composed of ice crystals is placed in the upper troposphere, so that its top is near -53°C, the tropopause temperature in the assumed background sounding. As a test, the cloud-top height was varied between -40° and -60°C, but the 3.9-μm reflectivities were insensitive to its location. Further details of the assumed background sounding are not discussed here since gaseous absorption is very limited above the cold clouds tops, even though absorption by gases is explicitly calculated in the model. Following the results from Baum et al. (2005a), the following mixture of ice crystal habits is assumed: $D_{\max} < 60$ μm is 100% droxtals; $60 < D_{\max} < 1000$ μm is 15% three-dimensional bullet rosettes, 50% solid columns, and 35% plates; $1000 < D_{\max} < 2000$ μm is 45% hollow columns, 45% solid columns, and 10% aggregates; $D_{\max} > 2000$ μm is 97% three-dimensional bullet rosettes and 3% aggregates, where $D_{\max}$ is the particle maximum dimension. For each calculation, we assume a gamma size distribution of the form

$$N(D) = AD^{\alpha}e^{-bD}, \tag{1}$$

where D is the equivalent volume spherical diameter, α is the shape parameter, and b is adjusted iteratively to achieve a desired effective radius. The shape parameter was chosen to be 1; a sensitivity analysis of this choice appears in section 3. Effective radius (r_e) is defined as

$$r_e = \frac{3}{4}\frac{\int_{D_{\mathrm{MIN}}}^{D_{\mathrm{MAX}}} V(D)N(D)\,dD}{\int_{D_{\mathrm{MIN}}}^{D_{\mathrm{MAX}}} A(D)N(D)\,dD}, \tag{2}$$

where $V(D)$ is the ice crystal volume and $A(D)$ is the crystal projected area (Yang et al. 2000). For a chosen effective radius, we use the habit mixture described above to obtain the cloud's net optical properties, namely, extinction, single scattering albedo, and scattering phase function (which is represented with a Legendre polynomial having 2500 terms) by weighting these optical properties based on the appropriate habit mixture. Note that a distribution having an effective radius of, say, 24 μm will include crystals having a maximum dimension up to ~200 μm (Fig. 1, top axis), so it would include droxtals, three-dimensional bullet rosettes, solid columns, and plates. Optical properties for these habits were obtained from Yang et al. (2005) by averaging over the spectral range of the GOES 3.9-μm band (3.78–4.03 μm). To handle the forward scattering peak, the phase functions have been modified by convolving the portions with scattering angles less than 10° by a Gaussian with 0.25° rms width, and by adjusting the forward peak height to normalize each phase func-

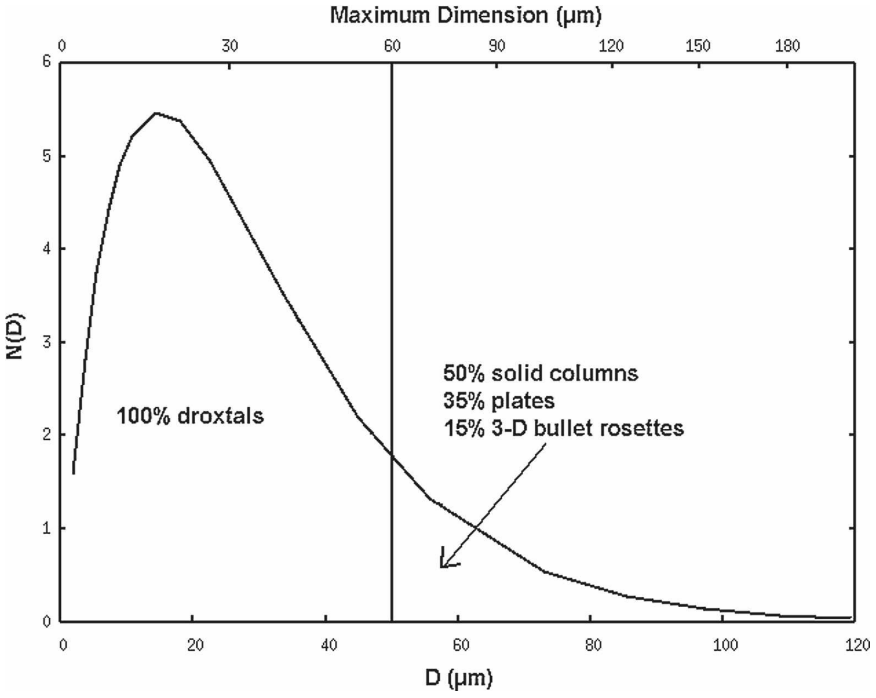

FIG. 1. Example gamma distribution for an effective radius of 24 μm. The axis on the bottom is equivalent volume spherical diameter (D); the axis on the top is ice crystal maximum dimension ($D_{\max}$). The vertical line at $D_{\max} = 60$ μm represents the cutoff between the particle mixtures described in the text.

tion. The extinction efficiency, single scattering albedo, and asymmetry parameter were then delta rescaled to maintain consistency. These optical properties were used along with solar geometry information (solar zenith angle and scattering angle) by SHDOMPP to calculate the expected satellite radiance for the GOES 3.9-μm band. The 10.7-μm brightness temperature is also calculated, so that 3.9-μm reflectivity ($\alpha_{3.9}$) can be determined using this relationship, derived for instance in Lindsey et al. (2006),

$$\alpha_{3.9} = \frac{R_{3.9} - R_{e_{3.9}}(T)}{S - R_{e_{3.9}}(T)}, \tag{3}$$

where $R_{3.9}$ is the total radiance at the band centered at 3.9 μm, $R_{e_{3.9}}(T)$ is the blackbody radiance at 3.9 μm with temperature T (which is estimated using the 10.7-μm brightness temperature), and S is the solar flux at the top of the atmosphere. Here $R_{e_{3.9}}(T)$ is computed without taking into account the channel filter function; however, for the cold clouds targeted by this retrieval, the blackbody radiance is quite small compared to the total radiance, so any error associated with neglecting the channel filter function is negligible.

Note that a GOES retrieval of $\alpha_{3.9}$ requires that the cloud optical depth be sufficiently large to prevent transmission of 3.9-μm radiation from below. Therefore, we limit our retrieval to pixels whose 10.7-μm brightness temperature is colder than -40°C, minimizing cloud transmissivity (Lindsey et al. 2006). An additional requirement is enforced to screen for optically thin clouds: the visible channel (0.65 μm) reflectance must exceed a critical value. To obtain a consistent visible reflectance from each satellite, GOES sensor degradation must be taken into account. A correction obtained from the National Environmental Satellite, Data, and Information Service (NESDIS) was applied to *GOES-10* (formally GOES-West) and *GOES-12* (currently GOES-East) radiances. A similar correction is not currently known for *GOES-11* (currently GOES-West), so we calculated the mean visible reflectance for all pixels colder than -40°C from July 2006, then determined a correction factor (1.12) to force the mean value to match the *GOES-12* mean value; this factor was then applied to all *GOES-11* visible reflectances. Finally, each visible reflectance was divided by the cosine of the solar zenith angle in order to approximate a reflectance value if the sun were directly overhead. The critical value of visible reflectance for sufficient optical depth was chosen to be 0.60. This value maximized the statistical measures described below in sections 3b and 3c.

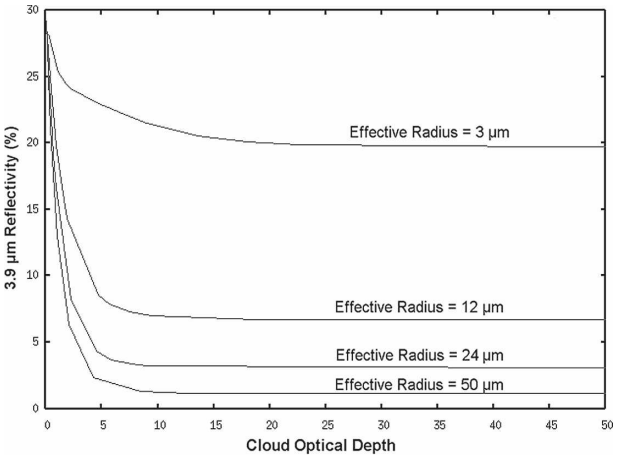

FIG. 2. Forward model calculations of 3.9-μm reflectivity as effective radius and cloud 3.9-μm optical depth are varied. A solar zenith angle of 17° and a scattering angle of 136° have been assumed.

To determine the model's sensitivity to optical depth, $\alpha_{3.9}$ was calculated for a wide range of cloud optical depths for distributions having four effective radii; the result is given in Fig. 2. For 3.9-μm optical depths greater than 20, $\alpha_{3.9}$ changes very little in every distribution. This means the cloud is sufficiently optically thick to prevent transmission from below, ensuring that the model-calculated $\alpha_{3.9}$ is accurate. For the series of model runs described below, the cloud optical depth was chosen to be greater than 20 for every simulation.

A total of 1377 model runs were performed, in which effective radius was varied between 3 and 51 μm, and the solar zenith and scattering angles were varied to account for the most extreme values given the locations of the current GOES. To vary the effective radius, ice mass and number concentration were changed, but as noted above the optical depth was forced to exceed 20 in every run. Each model result was used to populate a lookup table, so that GOES 3.9-μm reflectivity measurements can be used along with solar and satellite geometry to unambiguously determine optically thick ice cloud effective radius values. The lookup table comprises 27 unique effective radii, and for each one, 51 different times–locations so that the scattering angle varies from 57° to 180°, and the solar zenith angle from 1° to 79°. A scattering angle of 57° represents approximately the smallest possible value given the locations of GOES-East (75°W longitude) and GOES-West (135°W longitude). For observed scattering angles–zenith angles–3.9-μm reflectivities falling between those in the lookup table, linear interpolation is used to obtain an effective radius value. An example of this product is provided in Fig. 3. Thunderstorms in western Nebraska have significantly smaller effective radii than those in central Iowa; possible reasons for such differences are discussed in Lindsey et al. (2006). Note the missing values near the core of the southernmost thunderstorm in western Nebraska (white pixels surrounded by blue); these pixels were screened out by the visible reflectance requirement. Although actual optical depths are likely quite large here, this area is in the shadow of a significant overshooting dome, so visible reflectances are quite small. We feel that including the visible channel thin cloud screen provides a necessary and important improvement to the retrieval, especially since the relative occurrence of shadowed areas is small. In addition, areas with shadows also have anomalously low 3.9-μm reflectivities, which results in an effective radius estimate that is too large, so screening out these areas may actually be beneficial.

3. Error analysis

Validation of an ice cloud effective radius retrieval is extremely difficult for several reasons. In situ aircraft observations of cirrus clouds are rare, and those that do exist often have measurement errors associated with them. In addition, remotely sensed cloud properties provide information about a pixel-sized average cloud area, while aircraft typically fly at a single altitude directly through a cloud. In other words, the aircraft's observations may not be representative of what the satellite detects. Possible sources of error in this retrieval include (but are not limited to) 1) an incorrect estimate of 3.9-μm reflectivity from GOES due to transmission from below or instrument noise, 2) three-dimensional scattering effects due to cloud heterogeneity, 3) the existence of a non-gamma size distribution, 4) incorrect habit mixture assumptions, and 5) imperfect scattering properties of each habit. We rely on the results of Baum et al. (2005a), who use all available observational results to prescribe the ice crystal habit mixture discussed above, to hopefully minimize some of these errors. Instead of direct comparison with observations, we will employ a number of indirect methods to estimate the retrieval error.

a. GOES imager instrument noise

Studies of the GOES imager noise levels indicate a 3.9-μm radiance error of ± 0.008 mW m^{-2} sr^{-1} cm (Hillger et al. 2003). Using this value with Eq. (3), we find the maximum corresponding 3.9-μm reflectivity error to be $\pm 0.45\%$ (at a solar zenith angle of 67°, the largest allowed value in the retrieval). Figure 4a shows the forward model results using a solar zenith angle of 67°

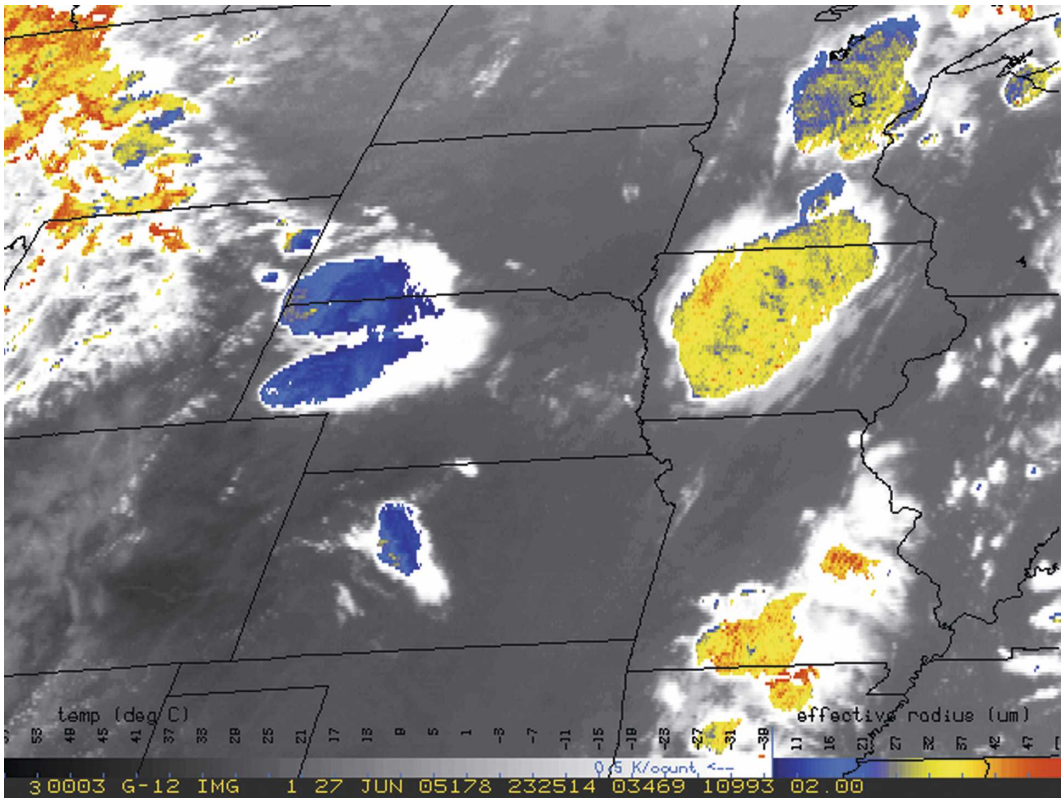

FIG. 3. *GOES-12* retrieval of effective radius for 10.7-μm brightness temperatures colder than -40°C (colors) and 10.7-μm brightness temperatures for warmer values (grayscale). Pixels colder than -40°C but with corrected visible reflectances less than 0.60 are forced to be white.

and a scattering angle of 131°. Scattering angle is defined as the angle formed between incoming solar radiation, a cloud, and the GOES satellite; 0° is in the forward direction, 180° backward. As shown in Fig. 4a, a 0.45% 3.9-μm reflectivity error leads to only a 0.5-μm effective radius error near 10 μm, but the signal deteriorates for larger effective radii, leading to an error near 10 μm for values near 45 μm. These results suggest that our retrieval is much more accurate for clouds with relatively small effective radii. Figure 4b shows the same curve as in Fig. 4a, along with two additional curves having different solar zenith and scattering angles. Each curve represents a different time at 30°N latitude, 105°W longitude on yearday 173. Notice that all three curves begin to flatten out at large effective radii, suggesting that the relatively large retrieval error should be expected for all locations and times of day.

b. Comparison with MODIS

Because of its horizontal resolution (1 km) and additional spectral bands, the MODIS instrument aboard the *Aqua* and *Terra* polar orbiters should be superior to GOES in retrieving cloud particle effective radius. It will therefore make a good basis for comparison. King et al. (2003) describe the MODIS effective radius retrieval algorithm used in the MODIS Level 2 Cloud Product. The most recent version of the Cloud Product (Collection 5) uses the exact same ice crystal habit assumptions as we employ (Yang et al. 2007), but the forward model used to generate the ice lookup tables is different [Discrete Ordinates Radiative Transfer model (DISORT; Stamnes et al. 1988)]. Additionally, gaseous absorption is neglected with the MODIS scheme in DISORT, but not in SHDOMPP. In the comparisons below, the MODIS effective radius was retrieved using band 7 (2.13 μm) and one of three possible nonabsorbing bands [band 1 (0.645 μm), band 2 (0.858 μm), or band 5 (1.24 μm)]. Absorption will be less with MODIS band 7 than with the GOES 3.9-μm band, particularly for the larger ice crystals (Platnick et al. 2003), so signal saturation at large effective radii should be minimal compared to GOES.

Eleven days from May and June of 2005, 2006, and 2007 were chosen in which at least one MODIS pass corresponded with a GOES scan over active deep convection in the continental United States. On two of the

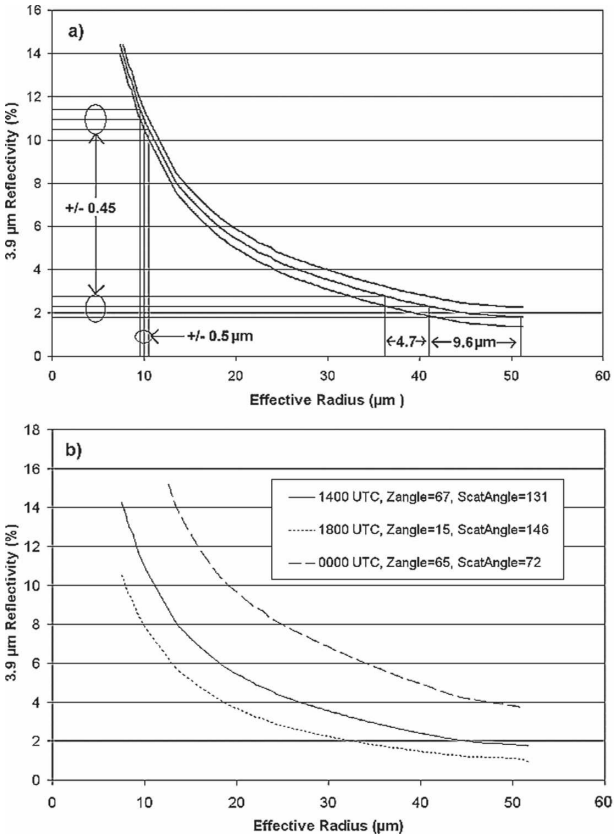

FIG. 4. Forward model results showing (a) the effect of a 0.45% 3.9-μm reflectivity error on the effective radius retrieval at 10 and 41 μm, and (b) the relationship between effective radius and 3.9-μm reflectivity for three times at Julian day 173 for a location at 30°N latitude, 105°W longitude.

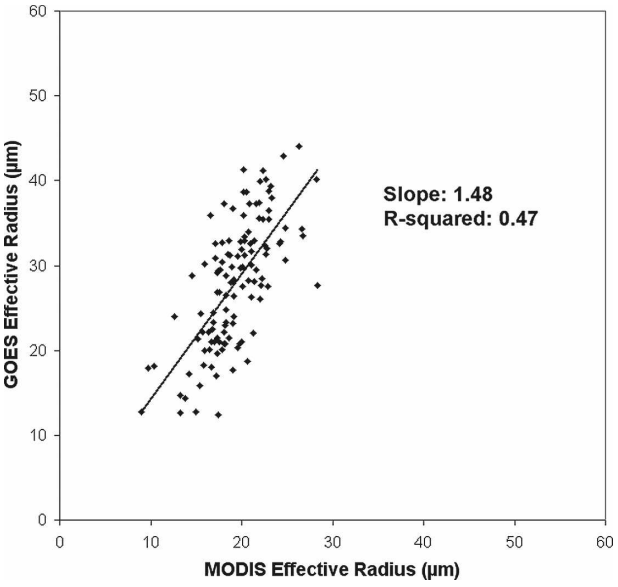

FIG. 5. Comparison of effective radius retrievals from MODIS and GOES. Each dot represents a mean effective radius from an individual cloud. The solid line represents the least squares linear best fit. The slope of the best-fit line and associated *R*-squared are indicated.

chosen days, two MODIS passes were selected, making a total of 13 MODIS passes for this analysis. Twelve of the 13 MODIS passes were by *Aqua*, the other by *Terra*. This is because *Aqua* passes over the continental United States latest each afternoon, increasing the chances that convection has begun. For each GOES scene, an algorithm was used to identify individual ice clouds (adjacent pixels having 10.7-μm brightness temperatures colder than −40°C and visible reflectance greater than 0.60), and each GOES pixel was matched (via latitude and longitude) with a corresponding array of the 25 nearest MODIS 1-km pixels. Effective radius values were averaged from these 25 MODIS pixels. It is quite rare for a MODIS scan time to match exactly with a GOES scan time at a given pixel, so a 5-min difference between scan times was allowed. Finally, GOES effective radius values from each pixel within every identified cloud were averaged, and the corresponding MODIS values were also averaged. By taking the cloud-averaged values, we hope to minimize any possible errors associated with the GOES–MODIS scan time differences. A total of 120 clouds were identified over the 11 days, and the result of the comparison is given in Fig. 5. Using a Student's *t* test, the resulting correlation (with correlation coefficient $r = 0.69$) is significant at a 99.9% confidence level. Note that the GOES-derived effective radius values tend to be larger than those from MODIS (a regression coefficient of 1.48). However, over 47% of the variance in the MODIS retrieval is explained by the best-fit curve, suggesting that despite its limitations in spatial and spectral resolution, GOES does a reasonable job of estimating thick cirrus cloud effective radius, at least compared to the MODIS algorithm.

Some of the differences between GOES and MODIS may be attributed to the GOES instrument noise described above in section 3a, but even at the smaller effective radii, the GOES-retrieved values tend to be a bit larger than those from MODIS. Other possible reasons for the observed differences include, but are not limited to the following: MODIS spatial resolution of 1 km allows smaller-scale cloud structure to be observed compared to GOES; the time difference between GOES and MODIS scans; differences in the development of the retrieval itself, including the use of the 3.9 μm band for GOES and the 2.13-μm band for MODIS, and using different radiative transfer models; errors in the calculation of 3.9-μm reflectivity with GOES; differences in the viewing geometries of MODIS and

GOES. Despite the differences, the ultimate goal of this retrieval is not to mimic that of MODIS, but rather to develop a reasonably accurate method that can be run in real time using GOES. Diurnal trends in cloud-top effective radius can be monitored, while the absolute value of the retrieved effective radius is not particularly important.

c. GOES-East–West comparison

A second indirect method to assess retrieval uncertainty makes use of the overlap in coverage of GOES-East and GOES-West over the central United States. This overlap allows near-simultaneous effective radius retrievals of a single cloud at two different scattering angles. If the independent retrievals turn out to be similar, it suggests that the assumed ice-crystal-scattering properties are reasonable. On the morning of 6 June 2005, thick cirrus clouds were observed between 110° and 95°W longitude over the United States, and numerous thunderstorms formed later in the day in the same region, many of which having very small effective radii. This day is an excellent choice for the comparison described above since 1) both GOES satellites were in RSO, providing many times for simultaneous scans, 2) observed thick cirrus clouds had a very wide range of effective radii, and 3) cirrus clouds occurred throughout the day, allowing for a wide range of solar zenith angles.

Starting at 1531 UTC and continuing to 2345 UTC, each time in which GOES-East and GOES-West scan times differed by no more than 2 min were identified (23 total; scattering angles vary from approximately 90° to 151°). At each time, an automated algorithm was used to locate every individual cloud having at least ten 10.7-μm pixels colder than -40°C and having a mean visible reflectance greater than 0.60. This cloud identification process was implemented for both GOES-East and GOES-West independently. The effective radius was retrieved for each pixel, and values were averaged for each cloud, providing a cloud mean effective radius. Corresponding clouds were identified, with care being taken to ensure the same cloud was being viewed by both satellites. Figure 6a is a scatterplot showing the 3.9-μm reflectivity of each cloud as viewed by the two satellites; the linear best-fit line and 1-to-1 line are provided for reference. The best-fit line in Fig. 6a has a slope of 0.54, indicating that GOES-East regularly measures larger 3.9-μm reflectivities than GOES-West since most of the convective clouds occurred in the afternoon hours, providing a forward-scattering direction for GOES-East. Both the slope and variance are significantly improved with the effective radius retrieval (Fig. 6b). This strong correlation between the GOES-East- and GOES-West-retrieved effective radii suggests that the assumed scattering properties perform quite well. The remaining variance could be associated with any number of potential errors, including those listed at the beginning of section 3, as well as slight calibration differences between *GOES-10* and *GOES-12*. Figure 6a is provided to show that using 3.9-μm reflectivity alone to infer effective radius would lead to

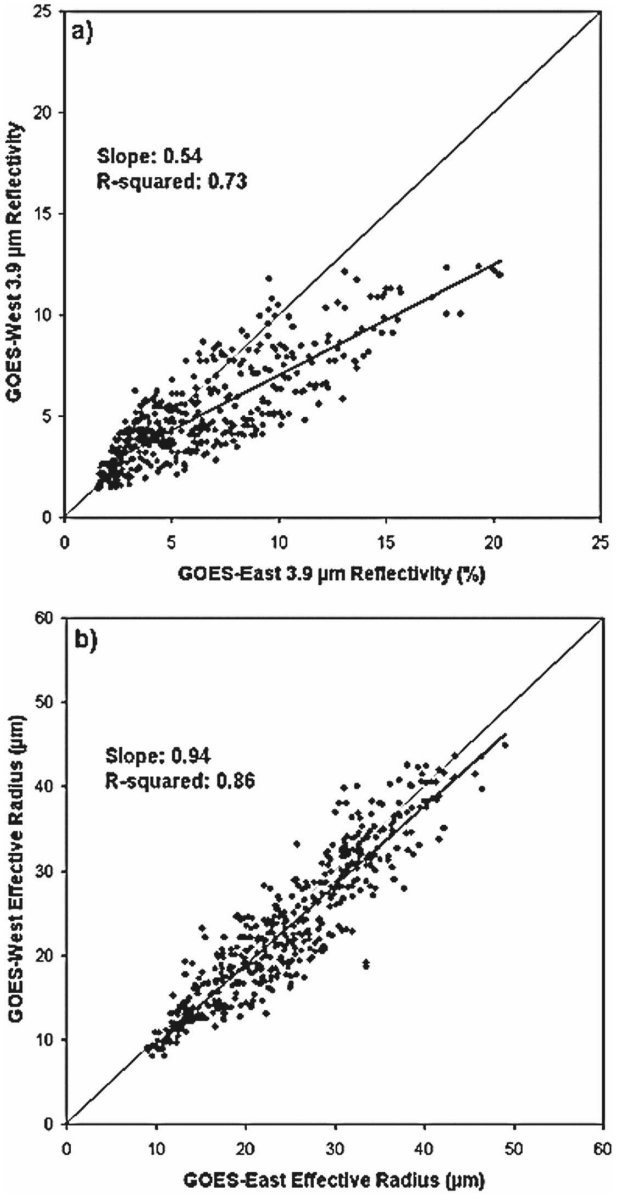

FIG. 6. GOES-East–/West comparison of (a) 3.9-μm reflectivity and (b) retrieved effective radius, from optically thick ice clouds occurring on 6 Jun 2005 between 1531 and 2345 UTC in the central United States. Both 3.9-μm reflectivities and effective radii were computed by averaging all pixel values for each cloud. The thick line is the least squares linear best fit; the thin line is the one-to-one line for reference. The slope of the best-fit line and associated *R*-squared are indicated.

significant errors, but taking into account the expected scattering properties of ice clouds and the sun-satellite geometry significantly improves the retrieval (Fig. 6b).

d. Shape parameter

One arbitrary choice when setting up the forward model runs was the gamma distribution's shape parameter [α in Eq. (1)], which we chose to be 1. To test the model's sensitivity to this parameter, 3.9-μm reflectivities were calculated for all effective radii using shape parameters of 0 and 4. The largest difference in 3.9-μm reflectivity occurs for an effective radius near 11 μm, a difference of 1.7%. This corresponds to an effective radius uncertainty of ± 2.0 μm at solar zenith angles approaching 70°; the uncertainty is lower for smaller zenith angles. Considering the wide range of effective radii observed (e.g., see Fig. 3), a maximum uncertainty of 2.0 μm at certain effective radii and solar zenith angles is not a concern. We chose $\alpha = 1$ as an intermediate value between the more extreme possibilities.

e. Effective radius climatology

In Lindsey et al. (2006), a map of mean summertime thick cirrus cloud 3.9-μm reflectivity is shown in their Fig. 2. It is noted that mean values as viewed from GOES-East and GOES-West differ over certain parts of the country, and the authors suggest that preferential forward scattering leads to the observed differences. Another way to test our effective radius retrieval is to redo this climatology and plot the mean effective radius rather than the mean 3.9-μm reflectivity. If the magnitudes and locations of maxima/minima agree, this lends more evidence that the assumed scattering properties are reasonable.

Figures 7a and 7b show the results of this climatology for May, June, July, and August of 2000, 2003, and 2004. Details on how the maps were generated are contained in Lindsey et al. (2006). Here, we have simply used the observed 3.9-μm reflectivities and solar and satellite geometry parameters along with the lookup tables described in section 2 to retrieve effective radius, before calculating the mean values. Notice that over the central United States, a minimum in mean effective radius is found in southeast Colorado and northeast New Mexico extending into the Texas Panhandle. The magnitude and location of this minimum is very similar as viewed from both GOES-East (Fig. 7a) and GOES-West (Fig. 7b). It should be noted that the visible reflectance thin cloud screen was not applied in making these maps because (i) it was not applied in Fig. 2 of Lindsey et al. (2006) and (ii) visible data over this period are not readily available. However, based on the results above, we feel that applying the screen will not significantly alter the results. The significant difference in mean effective radius between the high plains and the eastern United States is most likely related to the typical low-level thermodynamic environment in which thunderstorms form, as discussed in much more detail in Lindsey et al. (2006).

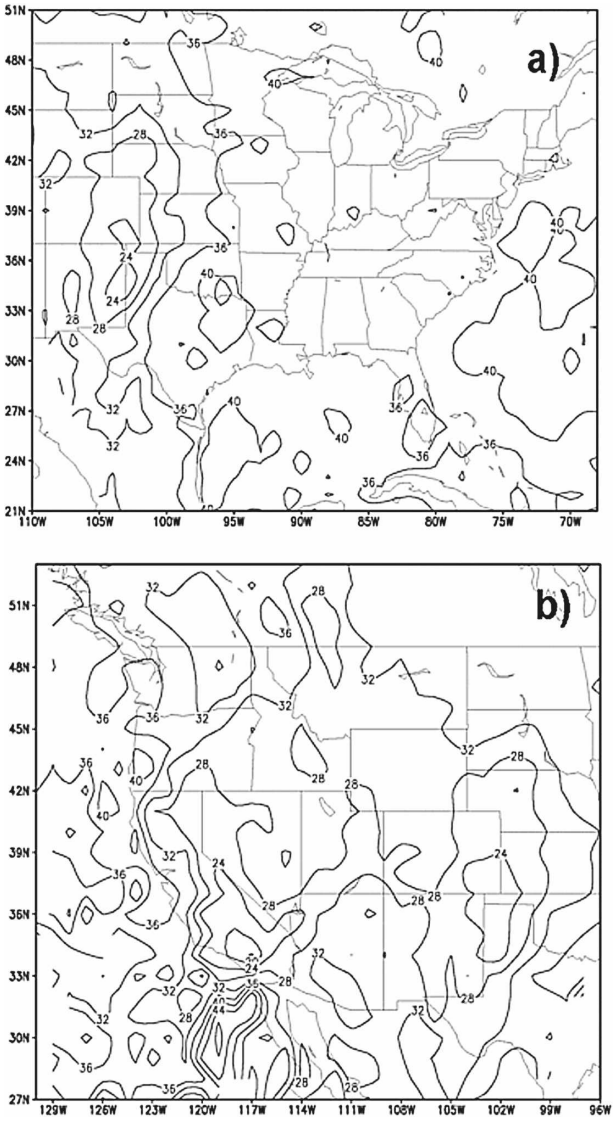

FIG. 7. Mean effective radius (μm) of ice clouds from (a) GOES-East and (b) GOES-West during May–Aug of 2000–2004, when the solar zenith angle was less than 68°. GOES-East covers much of the eastern continental United States, while GOES-West covers the western portion.

4. Summary

An effective radius retrieval has been developed for optically thick ice clouds using GOES. Forward model

calculations were performed using SHDOMPP, with cloud optical properties originating from scattering properties described by Yang et al. (2003, 2005). A mixture of ice crystal habits was assumed based on the crystal maximum dimension as suggested by Baum et al. (2005a). The forward model was used to generate 3.9-μm reflectivities for clouds having optical thicknesses greater then 20, and a large lookup table was populated by the model output. The GOES visible channel is used to screen for optically thin clouds, and bands centered at 3.9 and 10.7 μm are used to calculate 3.9-μm reflectivity. This measurement, along with solar geometry parameters, is used to identify the proper effective radius from the lookup table.

Since a direct validation of this method is impossible, we provide several indirect measures of the method's performance. First, information about the GOES 3.9-μm band's expected instrument error is used to estimate a maximum effective radius retrieval error of about 10 μm, but this error only occurs for the largest ice crystals. For smaller crystals, the error is less than 1 μm. Next, a comparison with MODIS-retrieved effective radius reveals that GOES does a reasonable job given its limitations. GOES values tend to be larger than those from MODIS, and over 47% of the variance in the MODIS retrieval is explained by a best-fit curve with the GOES values. We also tested the retrieval by obtaining effective radius values from the same cloud as viewed simultaneously by GOES-East and GOES-West. This analysis revealed that our assumed scattering properties are not perfect, but the scatter is minimal and the retrieval is a marked improvement over estimating effective radii using 3.9-μm reflectivity alone. A sensitivity analysis of the assumed gamma distribution's shape parameter was performed, and it was shown that a choice of $\alpha = 1$ can lead to a maximum error of ± 2 μm. It should be noted that additional error is likely associated with the gamma distribution assumption itself, since the actual distribution may be bimodal or highly irregular. Finally, a map of summertime mean effective radius of optically thick cirrus clouds was generated from both GOES-East and GOES-West, and locations and magnitudes of maxima and minima match quite well.

Work is currently under way to explain the observed differences in effective radius of convectively generated ice clouds. The excellent temporal resolution of GOES allows thunderstorm-top trends in ice crystal size to be monitored, and this may provide information about convective intensity changes. This application potentially makes our effective radius retrieval a useful tool for operationally forecasters.

Acknowledgments. This material is based on work supported by the National Oceanic and Atmospheric Administration under Grant NA67RJ0152. The authors thank Drs. Frank Evans, Chris Kummerow, Mark DeMaria, Don Hillger, Manajit Sengupta, and John Knaff for very insightful comments and discussion. In addition, the comments and suggestions from two anonymous reviewers significantly improved this manuscript. The views, opinions, and findings in this report are those of the authors and should not be construed as an official NOAA and/or U.S. government position, policy, or decision.

REFERENCES

Baum, B. A., A. J. Heymsfield, P. Yang, and S. T. Bedka, 2005a: Bulk scattering properties for the remote sensing of ice clouds. Part I: Microphysical data and models. *J. Appl. Meteor.,* **44,** 1885–1895.

——, P. Yang, A. J. Heymsfield, S. Platnick, M. D. King, Y.-X. Hu, and S. T. Bedka, 2005b: Bulk scattering properties for the remote sensing of ice clouds. Part II: Narrowband models. *J. Appl. Meteor.,* **44,** 1896–1911.

Cooper, S. J., T. S. L'Ecuyer, P. Gabriel, A. J. Baran, and G. L. Stephens, 2006: Objective assessment of the information content of visible and infrared radiance measurements for cloud microphysical property retrievals over the global oceans. Part II: Ice clouds. *J. Appl. Meteor. Climatol.,* **45,** 42–62.

Evans, K. F., 1998: The spherical harmonics discrete ordinate method for three-dimensional atmospheric radiative transfer. *J. Atmos. Sci.,* **55,** 429–446.

Grasso, L. D., and T. J. Greenwald, 2004: Analysis of 10.7-μm brightness temperatures of a simulated thunderstorm with two-moment microphysics. *Mon. Wea. Rev.,* **132,** 815–825.

Greenwald, T. J., R. Hertenstein, and T. Vukićević, 2002: An all-weather observational operator for radiance data assimilation with mesoscale forecast models. *Mon. Wea. Rev.,* **130,** 1882–1897.

Han, Q., W. B. Rossow, and A. A. Lacis, 1994: Near-global survey of effective droplet radii in liquid water clouds using ISCCP data. *J. Climate,* **7,** 465–497.

Hillger, D. W., T. J. Schmit, and J. M. Daniels, 2003: Imager and sounder radiance and product validations for the *GOES-12* science test. NOAA Tech. Rep. NESDIS 115, 70 pp.

King, M. D., and Coauthors, 2003: Cloud and aerosol properties, precipitable water, and profiles of temperature and water vapor from MODIS. *IEEE Trans. Geosci. Remote Sens.,* **41,** 442–458.

Lindsey, D. T., D. W. Hillger, L. Grasso, J. A. Knaff, and J. F. Dostalek, 2006: GOES climatology and analysis of thunderstorms with enhanced 3.9-μm reflectivity. *Mon. Wea. Rev.,* **134,** 2342–2353.

Liou, K.-N., 1986: Influence of cirrus clouds on weather and climate processes: A global perspective. *Mon. Wea. Rev.,* **114,** 1167–1199.

McKague, D., and K. F. Evans, 2002: Multichannel satellite retrieval of cloud parameter probability distribution functions. *J. Atmos. Sci.,* **59,** 1371–1382.

Minnis, P., K.-N. Liou, and Y. Takano, 1993: Inference of cirrus cloud properties using satellite-observed visible and infrared

radiances. Part I: Parameterization of radiance fields. *J. Atmos. Sci.,* **50,** 1279–1304.

Nakajima, T., and M. D. King, 1990: Determination of the optical thickness and effective particle radius of clouds from reflected solar radiation measurements. Part I: Theory. *J. Atmos. Sci.,* **47,** 1878–1893.

Platnick, S., M. D. King, S. A. Ackerman, W. P. Menzel, B. A. Baum, J. C. Riédi, and R. A. Frey, 2003: The MODIS cloud products: Algorithms and examples from Terra. *IEEE Trans. Geosci. Remote Sens.,* **41,** 459–473.

Roebeling, R. A., A. J. Feijt, and P. Stammes, 2006: Cloud property retrievals for climate monitoring: Implications of differences between Spinning Enhanced Visible and Infrared Imager (SEVIRI) on METEOSAT-8 and Advanced Very High Resolution Radiometer (AVHRR) on NOAA-17. *J. Geophys. Res.,* **111,** D20210, doi:10.1029/2005JD006990.

Stamnes, K., S.-C. Tsay, W. Wiscombe, and K. Jayaweera, 1988: Numerically stable algorithm for discrete-ordinate-method radiative transfer in multiple scattering and emitting layered media. *Appl. Opt.,* **27,** 2502–2509.

Stephens, G. L., S.-C. Tsay, P. W. Stackhouse Jr., and P. J. Flatau, 1990: The relevance of the microphysical and radiative properties of cirrus clouds to climate and climatic feedback. *J. Atmos. Sci.,* **47,** 1742–1753.

Wetzel, M. A., R. D. Borys, and L. E. Xu, 1996: Satellite microphysical retrievals for land-based fog with validation by balloon profiling. *J. Appl. Meteor.,* **35,** 810–829.

Yang, P., K. N. Liou, K. Wyser, and D. Mitchell, 2000: Parameterization of the scattering and absorption properties of individual ice crystals. *J. Geophys. Res.,* **105,** 4699–4718.

——, B. A. Baum, A. J. Heymsfield, Y. X. Hu, H.-L. Huang, S.-C. Tsay, and S. Ackerman, 2003: Single-scattering properties of droxtals. *J. Quant. Spectrosc. Radiat. Transfer,* **79-80,** 1159–1169.

——, H. Wei, H.-L. Huang, B. A. Baum, Y. X. Hu, G. W. Kattawar, M. I. Mishchenko, and Q. Fu, 2005: Scattering and absorption property database for nonspherical ice particles in the near- through far-infrared spectral region. *Appl. Opt.,* **44,** 5512–5523.

——, L. Zhang, G. Hong, S. L. Nasiri, B. A. Baum, H.-L. Huang, M. D. King, and S. Platnick, 2007: Differences between collection 4 and 5 MODIS ice cloud optical/microphysical products and their impact on radiative forcing simulations. *IEEE Trans. Geosci. Remote Sens.,* **45,** 2886–2899.